Reactive & Functional Polymers 86 (2015) 16–26

Contents lists available at ScienceDirect

Reactive & Functional Polymers

journal homepage: www.elsevier.com/locate/react

Towards continuous junction (CJ) organic electronic devices: Fast and clean post-polymerization modification by oxidation using dimethyldioxirane (DMDO)

Florian Glöcklhofer [a], Daniel Lumpi [a,*], Markus Kohlstädt [b,c], Olena Yurchenko [c,d], Uli Würfel [b,c], Johannes Fröhlich [a]

[a] Institute of Applied Synthetic Chemistry (IAS), Vienna University of Technology, Getreidemarkt 9/163, A-1060 Vienna, Austria
[b] Fraunhofer Institute for Solar Energy Systems (ISE), Heidenhofstrasse 2, D-79110 Freiburg, Germany
[c] Freiburg Materials Research Center (FMF), University of Freiburg, Stefan-Meier-Strasse 21, D-79104 Freiburg, Germany
[d] Institute of Microsystems Engineering (IMTEK), University of Freiburg, Georges Köhler-Allee 103, D-79110 Freiburg, Germany

ARTICLE INFO

Article history:
Received 4 June 2014
Received in revised form 2 September 2014
Accepted 26 October 2014
Available online 11 November 2014

Keywords:
Continuous junction
Post-polymerization modification
Dimethyldioxirane
Functional polymers
Organic electronics

ABSTRACT

An advanced design concept for organic electronic devices relying on functional polymers is presented. The concept aims at realizing a gradual transition from an electron-donating to an electron-accepting material in a specific post-polymerization modification step. Hence, this approach facilitates a straight forward fabrication compared to conventional multi-layer architectures. The synthesis via microwave-assisted Cu(I)-catalyzed azide–alkyne cycloaddition of the reactive polymers based on sulfur, selenium and tellurium as active sites is presented; full characterization of model compounds and polymers is provided. Additionally, a reliable procedure for post-polymerization oxidation applying dimethyldioxirane is developed. Photophysical and electrochemical characteristics of the novel polymers reveal the feasibility but also the challenges of the continuous junction concept.

1. Introduction

Modern organic light-emitting diodes (OLEDs) consist of several layers of materials [1]. While the central emitting layer serves as the primary site of electron–hole recombination, the adjacent hole and electron transporting layers as well as the hole and electron injection layers improve charge carrier transport and eliminate carrier leakage and exciton quenching [2].

In organic photovoltaic devices (OPVs) on the other hand, selective layers improve charge carrier extraction at the electrodes. In addition, prior to extraction two different materials – a donor and an acceptor phase – are required inside the photoactive layer for an efficient separation of the strongly bound electron–hole pairs known as excitons, generated upon illumination [3]. Due to the low dielectric constants in the organic components, exciton dissociation occurs almost exclusively at the donor–acceptor interface [4].

Today, polymer solar cells (PSCs) mainly rely on the bulk heterojunction (BHJ) concept: donor and acceptor material are blended prior to processing and form a bicontinuous interpenetration network within the active layer of the solar cell. This ensures a large surface area between the donor–acceptor interface and, thus, increases the probability for excitons to reach the interface within their limited lifetime [3,5].

However, improving charge separation and transport as well as enhancing the limited control of morphology still remain important issues in OPV development. One goal of current research is to achieve ordered structures within the organic layer of OPVs. Besides decreasing the distance between donor and acceptor material, this aims at solving morphology issues like inclusions, which hinder charge transport to the respective electrodes [6]. The graded donor–acceptor heterojunction concept for small molecules focuses on solving the same issue by a varying donor–acceptor composition across the active layer [7].

In this work, we propose a new approach which potentially enables to overcome the described issues and – in addition – is available by a straight forward procedure. We are aiming at realizing a gradual transition from an electron-donating to an electron-accepting material. The advantages of this novel conceptual

* Corresponding author. Tel.: +43 158801163719; fax: +43 15880115499.
E-mail addresses: florian.gloecklhofer@tuwien.ac.at (F. Glöcklhofer), daniel.lumpi@tuwien.ac.at (D. Lumpi), markus.kohlstaedt@ise.fraunhofer.de (M. Kohlstädt), olena.yurchenko@fmf.uni-freiburg.de (O. Yurchenko), uli.wuerfel@ise.fraunhofer.de (U. Würfel), johannes.froehlich@tuwien.ac.at (J. Fröhlich).

http://dx.doi.org/10.1016/j.reactfunctpolym.2014.10.006
1381-5148/

design for organic electronic devices as well as the intended steps of device fabrication are discussed in detail.

In addition, functional electron-donor polymers suitable for post-polymerization modification allowing for such a continuous junction (CJ) concept were developed and are presented.

The CJ concept and, therefore, the developed materials are of relevance for a broad community in the field of organic electronics. In addition to OPV applications, the CJ concept also represents a valuable strategy in OLED fabrication and may significantly simplify the current multi-layer device architecture.

2. Experimental

2.1. Materials

Oxidizable substituents – preferably chalcogenide substituents – attached to a conjugated polymer backbone are required for post-polymerization modification using DMDO. However, common materials for OLED and OPV devices do not feature sulfide, selenide or telluride substituents. Therefore, we recently reported on a scalable synthesis of building blocks **1a–c** for such polymers [8]. Azide–alkyne cycloaddition allows for a simple functionalization of such alkynes and therefore was the choice of reaction for the synthesis of model compounds **3aa–cb** and polymers **6aa–cb** bearing oxidizable substituents.

The materials were developed to demonstrate functionalization of the novel building blocks and to demonstrate efficient material modification by applying DMDO. Azidobenzene **2a** and 4-azido-*N,N*-dimethylaniline **2b** were used for the synthesis of small molecules (Scheme 1) due to structural similarity to diazides **5a** and **5b**, which were used for polymerization.

Oxidation using DMDO has been investigated for the synthesis of **4aa** and **4ab** (Scheme 2). Dimethyldioxirane (DMDO) is of particular interest for this modification since it enables a stepwise conversion of electronic properties by inversion of electron-donating groups into electron-accepting moieties. This reagent, which can be prepared efficiently on a large laboratory scale [9], fulfills all criteria for a successful realization of a gradual transition from a donor to an acceptor material within a PSC.

Fluorene and carbazole based diazides **5a** and **5b** were chosen for AA–BB polymerization (Scheme 3). These two structural units are commonly applied in organic electronic materials [10]. Solubility issues are the reason for applying branched side-chains

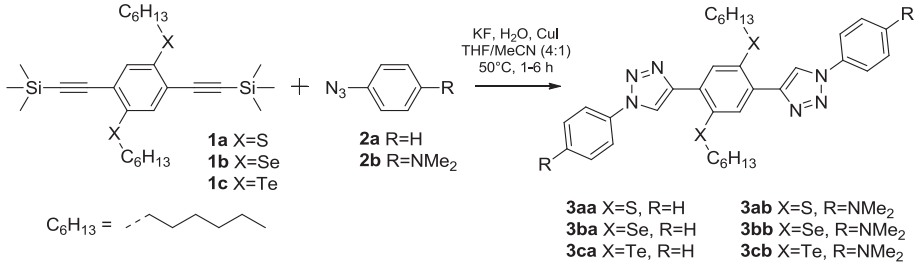

Scheme 1. Model compounds **3aa–3cb**: Synthesis and molecular structure.

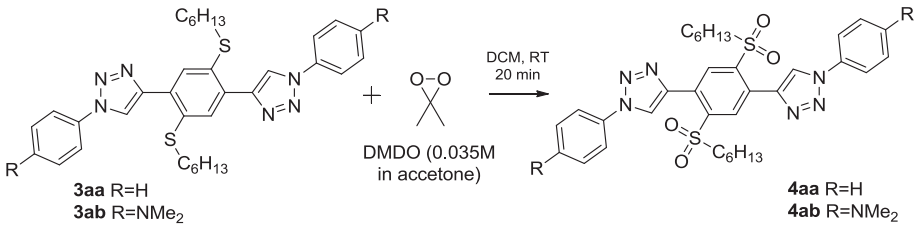

Scheme 2. Model compounds **4aa** and **5ab**: Oxidation using dimethyldioxirane (DMDO).

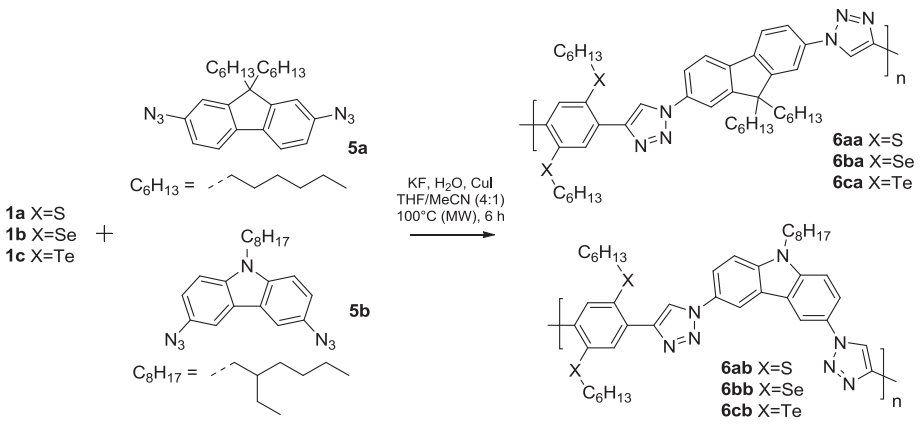

Scheme 3. Polymers **6aa–cb**: AA–BB polymerization of dialkynes **1a–c** and diazides **5a–b**.

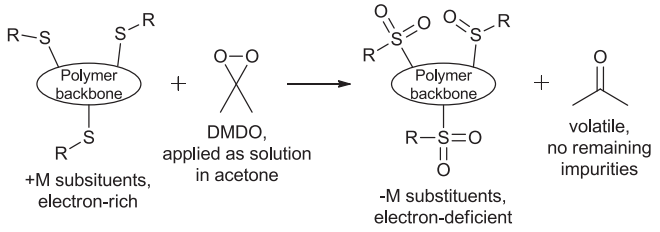

Scheme 4. General process of post-polymerization modification using DMDO.

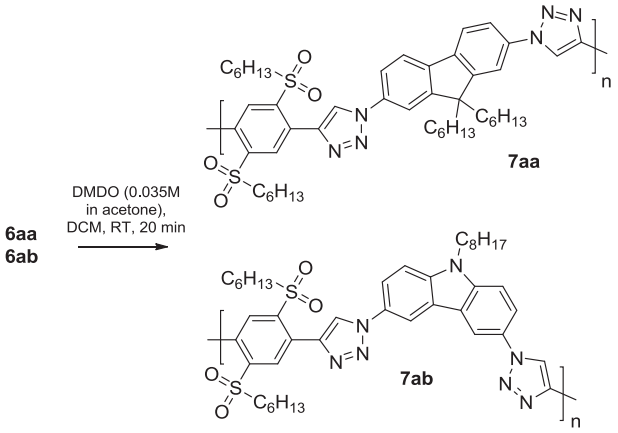

Scheme 5. Polymers **7aa** and **7ab**: Post-polymerization modification using dimethyldioxirane (DMDO).

for the carbazole derivatives since the carabzole based polymers utilizing linear side-chains show low solubility rendering spin-coating processing impossible. Polymerization was carried out in a microwave reactor in order to reduce reaction times.

Oxidation of the obtained polymers (the general reaction is illustrated in Scheme 4) **6aa** and **6ab** (Scheme 5) was carried out under the same conditions as the synthesis of **4aa** and **4ab**.

2.2. Instrumentation and device fabrication

NMR spectra were recorded at 200 MHz for ^{1}H and 50 MHz for ^{13}C on a Bruker Avance 200 or at 400 MHz for ^{1}H and 100 MHz for ^{13}C on a Bruker Avance DRX-400 Spectrometer in case of low solubility. Data for ^{1}H NMR are reported as follows: chemical shift in parts per million from TMS (tetramethylsilane) with the residual solvent signal as an internal reference ($CDCl_3$ δ = 7.26 ppm, CD_2Cl_2 δ = 5.32 ppm), multiplicity (s = singlet, d = doublet, t = triplet and m = multiplet; br = broad), coupling constant in Hz and integration. ^{13}C NMR spectra are reported in ppm from TMS using the central peak of the solvent as reference ($CDCl_3$ δ = 77.0 ppm, CD_2Cl_2 δ = 54.0 ppm), multiplicity with respect to proton (deduced from APT experiments, s = quaternary C, d = CH, t = CH_2, q = CH_3).

Microwave-assisted reactions were carried out in a BIOTAGE Initiator EXP EU 355301 microwave reactor. Pre-stirring was set to 10 s, fixed hold time and cooling-while-heating (cwh) was applied.

HR-MS data was obtained from matrix-assisted laser desorption/ionization (MALDI) measurements using a system provided by Thermo Scientific (MALDI LTQ Orbitrap and LTQ Orbitrap XL). α-Cyano-4-hydroxycinnamic acid (CHCA) was applied as matrix for all given HR-MS measurements.

UV/VIS absorption spectra in solution were recorded on a Perkin Elmer Lambda 750 using Suprasil glass cuvettes. The measurements were performed of sample solutions in dry DCM (5 μM (concentration of polymer repeating units)) at room temperature. UV/VIS absorption spectra of polymer thin films were recorded with a Perkin Elmer Lambda 40 UV/VIS spectrometer equipped with a solid sample holder.

The fluorescence spectra were recorded on an Edinburgh FLS920 system using Suprasil glass cuvettes. The measurements were performed of sample solutions in dry DCM (5 μM (concentration of polymer repeating units)) at room temperature. Quantum yields of polymers were determined on the same system using a spherical setup (Ulbricht sphere). The measurements were also performed in dry DCM (5 μM and additionally at 50 μM for all measured polymers and 500 μM as well as 5000 μM for **6aa** to further investigate concentration dependence).

Gel permeation measurements were carried out in THF (with the exception of polymer **6ca** which was measured in $CHCl_3$ due to poor solubility in THF) on a Waters/Viscotek system (Waters 515 HPLC pump, Waters 717plus autosampler, Waters 2410 RI detector, Waters temperature Controller, OmniSec Software) equipped with three columns (Styragel HR 0.5 THF, Styragel HR 3 THF, Styragel HR 4 THF). Polystyrene standards were used for calibration.

Differential scanning calorimetry (DSC) measurements were carried out at a heating rate of 10 K min^{-1} in a flowing argon atmosphere (25 ml min^{-1}) on a Netsch DSC 200 F3 Maia, working with aluminum pans with pierced lids.

Cyclic voltammetry experiments were performed with an AutoLab Potentiostat–Galvanostat PGSTAT30 on polymer films in acetonitrile containing 0.1 M tetra-n-butylammonium hexafluorophosphate as supporting electrolyte at a scan rate of 20 mV/s. The Ag/AgCl wire was used as a reference electrode, platinum sheets as counter and working electrode. The working electrode was covered with a thin polymer film by spin coating from chloroform solution. Prior to experiments, the electrochemical cell was dried by vacuum pumping at 300 °C for 2 h and filling with dry argon. The reference electrode was calibrated at the end of experiments with the redox couple ferrocene/ferrocenium [$E_{1/2}$(Fc/Fc$^+$ vs Ag/AgCl) = 0.37 V].

For the fabrication of organic field effect transistors (OFETs), P-doped silicon substrates were surface passivated by thermal oxidation forming SiO_2 and used as substrates. Interdigitating source and drain electrodes were fabricated by subsequent evaporation of 10 nm chromium and 100 nm gold. Polymers were deposited on top of these structures by spin-coating a solution (20 mg/mL in chlorobenzene) after filtering through a 0.45 μm PTFE syringe filter, resulting in layer thicknesses of approx. 80 nm. The channel length was varied between 5 and 20 μm, while the ratio between channel width (W) and channel length (L) was kept constant (W/L = 7200). The samples were annealed at 120 °C for 10 min before measurement of the OFET characteristics. Additionally, the influence of different annealing temperatures (no annealing, 60 °C, 90 °C, 120 °C, 200 °C, 10 min annealing time each), light/dark conditions during measurement and 10 min exposure to air shortly before measuring were tested for polymer **6ba**. Unless otherwise noted, all steps were performed in a nitrogen-filled glovebox. Output characteristics of the OFETs were measured at gate–source voltages from −60 V to 0 V, transfer characteristics measured at drain–source voltages at 0 V and −60 V, without illumination and under inert atmosphere, unless otherwise noted. Measurements were taken using two synchronized Keithley model 2400 source measure units. For the construction of polymer diodes, prepatterned ITO-substrates were cleaned twice in acetone, isopropanol and subsequently water under ultrasonic agitation for 5 min each, blow dried with nitrogen and UV–ozone treated for 20 min. A 40 nm thick PEDOT:PSS layer was spin-coated onto the substrates which were then annealed at 130 °C for 10 min. All subsequent steps have been performed under nitrogen atmosphere. Polymers were deposited by spin-coating a solution (20 mg/mL in chlorobenzene) after filtering through a 0.45 μm PTFE syringe filter. The polymer layers were

annealed at 120 °C for 10 min. The layer stack was completed by thermal evaporation of 100 nm calcium, defining the active area of the devices (0.09 cm^2). Current–voltage curves were measured using a Keithley 2400 source meter and under simulated AM1.5G illumination (1000 W/m^2).

2.3. Synthesis

All reactions were performed in oven-dried glassware. Reagents were purchased from common commercial sources and used without further purification. Anhydrous solvents were prepared by filtration through drying columns.

Dialkynes **1a–c** [8], azides **2a** [11] and **2b** [12], dimethyldioxirane (DMDO) [9] and diazides **5a** [13] and **5b** [8] were synthesized according to published procedures. Syntheses and characterizations of polymers **6ab** and **7ab** were reported as preliminary results in a previous work [8] and are added for completeness.

2.3.1. *General procedure for the azide–alkyne cycloaddition towards 3aa–cb*

1a–c (1.0 eq), **2a/b** (2.2 eq), KF (3.0 eq), water (4.0 eq) and CuI (10 mol%) were dissolved in degassed THF/MeCN (4:1, 0.1 M). The solution was heated to 50 °C and stirred for 1–6 h until TLC analysis indicated complete conversion. The reaction was then poured on water and extracted three times with DCM. The combined organic layers were dried over anhydrous Na_2SO_4 and the solvent was removed in vacuo. The solid residue was then triturated in boiling EtOH. After cooling to room temperature the desired compound was obtained by vacuum filtration.

2.3.1.1. *4,4′-[2,5-Bis(hexylthio)-1,4-phenylene]bis[1-phenyl-1H-1,2,3-triazole] 3aa*. **1a** (251.5 mg, 0.50 mmol, 1.0 eq), **2a** (131.0 mg, 1.10 mmol, 2.2 eq), KF (87.2 mg, 1.50 mmol, 3.0 eq), H_2O (36.0 mg, 2.00 mmol, 4.0 eq) and CuI (9.5 mg, 0.05 mmol, 10 mol%) in 5 ml THF/MeCN (4:1, 0.1 M) were heated to 50 °C for 6 h. Trituration in 8 ml boiling EtOH and following vacuum filtration yielded 191.4 mg (0.321 mmol, 64%) of the orange solid **3aa**. ^{1}H NMR (200 MHz, $CDCl_3$): δ = 8.77 (s, 2H), 8.31 (s, 2H), 7.84 (d, J = 8.0 Hz, 4H), 7.62–7.44 (m, 6H), 3.04 (t, J = 7.3 Hz, 4H), 1.69 (quint, J = 7.3 Hz, 4H), 1.50–1.22 (m, 12H), 0.85 (t, J = 6.5 Hz, 6H) ppm. ^{13}C NMR (50 MHz, $CDCl_3$): δ = 145.3 (s), 137.1 (s), 132.5 (s), 130.2 (s), 130.0 (d), 129.8 (d), 128.8 (d), 121.7 (d), 120.6 (d), 34.3 (t), 31.3 (t), 28.7 (t), 28.6 (t), 22.5 (t), 14.0 (q) ppm. Anal Calcd for $C_{34}H_{40}N_6S_2$: *m/z* 597.2836 $[M + H]^+$. Found: MS (MALDI, CHCA): *m/z* 597.2841 $[M + H]^+$.

2.3.1.2. *4,4′-[2,5-Bis(hexylseleno)-1,4-phenylene]bis[1-phenyl-1H-1,2,3-triazole] 3ba*. **1b** (298.4 mg, 0.50 mmol, 1.0 eq), **2a** (131.0 mg, 1.10 mmol, 2.2 eq), KF (87.2 mg, 1.50 mmol, 3.0 eq), H_2O (36.0 mg, 2.00 mmol, 4.0 eq) and CuI (9.5 mg, 0.05 mmol, 10 mol%) in 5 ml THF/MeCN (4:1, 0.1 M) were heated to 50 °C for 5 h. Trituration in 10 ml boiling EtOH and following vacuum filtration yielded 217.3 mg (0.315 mmol, 63%) of the yellow–orange solid **3ba**. ^{1}H NMR (200 MHz, $CDCl_3$): δ = 8.66 (s, 2H), 8.20 (s, 2H), 7.82 (d, J = 7.5 Hz, 4H), 7.59–7.39 (m, 6H), 2.99 (t, J = 7.3 Hz, 4H), 1.70 (quint, J = 7.3 Hz, 4H), 1.45–1.19 (m, 12H), 0.82 (t, J = 6.3 Hz, 6H) ppm. ^{13}C NMR (50 MHz, $CDCl_3$): δ = 146.4 (s), 136.9 (s), 133.3 (d), 132.0 (s), 129.8 (d), 128.8 (d), 128.5 (s), 121.0 (d), 120.5 (d), 31.2 (t), 29.5 (t), 29.4 (t), 29.1 (t), 22.5 (t), 13.9 (q) ppm. Anal Calcd for $C_{34}H_{40}N_6Se_2$: *m/z* 693.1725 $[M + H]^+$. Found: MS (MALDI, CHCA): *m/z* 693.1742 $[M + H]^+$.

2.3.1.3. *4,4′-[2,5-Bis(hexyltelluro)-1,4-phenylene]bis[1-phenyl-1H-1,2,3-triazole] 3ca*. **1c** (347.0 mg, 0.50 mmol, 1.0 eq), **2a** (131.0 mg, 1.10 mmol, 2.2 eq), KF (87.2 mg, 1.50 mmol, 3.0 eq), H_2O (36.0 mg, 2.00 mmol, 4.0 eq) and CuI (9.5 mg, 0.05 mmol, 10 mol%) in 5 ml THF/MeCN (4:1, 0.1 M) were heated to 50 °C for 1 h. Trituration in 20 ml boiling EtOH and following vacuum filtration yielded 210.6 mg (0.267 mmol, 53%) of the orange solid **3ca**. ^{1}H NMR (200 MHz, $CDCl_3$): δ = 8.37 (s, 2H), 7.98 (s, 2H), 7.81 (d, J = 7.4 Hz, 4H), 7.59–7.46 (m, 6H), 2.88 (t, J = 7.4 Hz, 4H), 1.79 (quint, J = 7.1 Hz, 4H), 1.40–1.18 (m, 12H), 0.82 (t, J = 6.1 Hz, 6H) ppm. ^{13}C NMR (50 MHz, $CDCl_3$): δ = 148.6 (s), 136.8 (s), 135.8 (d), 134.4 (s), 129.7 (d), 128.8 (d), 120.4 (d), 119.5 (d), 113.8 (s), 31.8 (t), 31.2 (t), 30.5 (t), 22.5 (t), 14.0 (q) ppm. Anal Calcd for $C_{34}H_{40}N_6Te_2$: *m/z* 793.1519 $[M + H]^+$. Found: MS (MALDI, CHCA): *m/z* 793.1543 $[M + H]^+$.

2.3.1.4. *4,4′-[2,5-Bis(hexylthio)-1,4-phenylenebis(1H-1,2,3-triazole-4,1-diyl)]bis[N,N-dimethylbenzeneamine] 3ab*. **1a** (251.5 mg, 0.50 mmol, 1.0 eq), **2b** (178.4 mg, 1.10 mmol, 2.2 eq), KF (87.2 mg, 1.50 mmol, 3.0 eq), H_2O (36.0 mg, 2.00 mmol, 4.0 eq) and CuI (9.5 mg, 0.05 mmol, 10 mol%) in 5 ml THF/MeCN (4:1, 0.1 M) were heated to 50 °C for 4 h. Trituration in 12 ml boiling EtOH and following vacuum filtration yielded 265.6 mg (0.389 mmol, 78%) of the red solid **3ab**. ^{1}H NMR (200 MHz, $CDCl_3$): δ = 8.62 (s, 2H), 8.28 (s, 2H), 7.64 (d, J = 9.0 Hz, 4H), 6.81 (d, J = 9.1 Hz, 4H), 3.04 (s, 12H), 3.02 (t, J = 7.3 Hz, 4H), 1.67 (quint, J = 7.3 Hz, 4H), 1.48–1.19 (m, 12H), 0.85 (t, J = 6.4 Hz, 6H) ppm. ^{13}C NMR (50 MHz, $CDCl_3$): δ = 150.6 (s), 144.9 (s), 132.3 (s), 130.4 (s), 129.9 (d), 126.8 (s), 122.0 (d), 112.3 (d), 40.5 (q), 34.3 (t), 31.3 (t), 28.7 (t), 28.6 (t), 22.5 (t), 14.0 (q) ppm. Anal Calcd for $C_{38}H_{50}N_8S_2$: *m/z* 683.3680 $[M + H]^+$. Found: MS (MALDI, CHCA): *m/z* 683.3689 $[M + H]^+$.

2.3.1.5. *4,4′-[2,5-Bis(hexylseleno)-1,4-phenylenebis(1H-1,2,3-triazole-4,1-diyl)]bis[N,N-dimethylbenzeneamine] 3bb*. **1b** (298.4 mg, 0.50 mmol, 1.0 eq), **2b** (178.4 mg, 1.10 mmol, 2.2 eq), KF (87.2 mg, 1.50 mmol, 3.0 eq), H_2O (36.0 mg, 2.00 mmol, 4.0 eq) and CuI (9.5 mg, 0.05 mmol, 10 mol%) in 5 ml THF/MeCN (4:1, 0.1 M) were heated to 50 °C for 5 h. Trituration in 15 ml boiling EtOH and following vacuum filtration yielded 225.1 mg (0.290 mmol, 58%) of the red solid **3bb**. ^{1}H NMR (200 MHz, $CDCl_3$): δ = 8.49 (s, 2H), 8.17 (s, 2H), 7.62 (d, J = 9.0 Hz, 4H), 6.79 (d, J = 9.1 Hz, 4H), 3.02 (s, 12H), 2.96 (t, J = 7.4 Hz, 4H), 1.70 (quint, J = 7.4 Hz, 4H), 1.45–1.19 (m, 12H), 0.83 (t, J = 6.5 Hz, 6H) ppm. ^{13}C NMR (50 MHz, $CDCl_3$): δ = 150.5 (s), 146.0 (s), 133.0 (d), 132.2 (s), 128.3 (s), 126.6 (s), 121.9 (d), 121.0 (d), 112.3 (d), 40.4 (q), 31.2 (t), 29.5 (t), 29.3 (t), 28.7 (t), 22.5 (t), 14.0 (q) ppm. Anal Calcd for $C_{38}H_{50}N_8Se_2$: *m/z* 779.2569 $[M + H]^+$. Found: MS (MALDI, CHCA): *m/z* 779.2587 $[M + H]^+$.

2.3.1.6. *4,4′-[2,5-Bis(hexyltelluro)-1,4-phenylenebis(1H-1,2,3-triazole-4,1-diyl)]bis[N,N-dimethylbenzeneamine] 3cb*. **1c** (347.0 mg, 0.50 mmol, 1.0 eq), **2b** (178.4 mg, 1.10 mmol, 2.2 eq), KF (87.2 mg, 1.50 mmol, 3.0 eq), H_2O (36.0 mg, 2.00 mmol, 4.0 eq) and CuI (9.5 mg, 0.05 mmol, 10 mol%) in 5 ml THF/MeCN (4:1, 0.1 M) were heated to 50 °C for 3 h. Trituration in 15 ml boiling EtOH and following vacuum filtration yielded 290.1 mg (0.332 mmol, 66%) of the orange solid **3cb**. ^{1}H NMR (200 MHz, $CDCl_3$): δ = 8.19 (s, 2H), 7.91 (s, 2H), 7.61 (d, J = 9.0 Hz, 4H), 6.78 (d, J = 9.0 Hz, 4H), 3.03 (s, 12H), 2.86 (t, J = 7.4 Hz, 4H), 1.80 (quint, J = 7.3 Hz, 4H), 1.45–1.21 (m, 12H), 0.83 (t, J = 6.3 Hz, 6H) ppm. ^{13}C NMR (50 MHz, $CDCl_3$): δ = 150.6 (s), 148.3 (s), 135.4 (d), 134.6 (s), 126.6 (s), 121.9 (d), 119.1 (d), 113.5 (s), 112.3 (d), 40.5 (q), 31.9 (t), 31.2 (t), 30.7 (t), 22.5 (t), 14.0 (q) ppm. Anal Calcd for $C_{38}H_{50}N_8Te_2$: *m/z* 879.2363 $[M + H]^+$. Found: MS (MALDI, CHCA): *m/z* 879.2391 $[M + H]^+$.

2.3.2. *General oxidation procedure towards 4aa and 4ab*

3aa/**3ab** (1.0 eq) was dissolved in DCM (0.008 M). DMDO (0.035 M in acetone, 4.0 eq) was added dropwise and the solution

stirred for 20 min at room temperature. Simple evaporation of the solvents yielded the desired products.

2.3.2.1. ***4,4′-[2,5-Bis(hexylsulfonyl)-1,4-phenylene]bis[1-phenyl-1H-1,2,3-triazole] 4aa.*** **3aa** (59.7 mg, 0.1 mmol, 1.0 eq) in 12.5 ml DCM (0.008 M) and 11.4 ml DMDO (0.035 M in acetone, 0.4 mmol, 4 eq). 65.5 mg (0.099 mmol, 99%) of **4aa** were obtained as a slightly yellow solid. ^{1}H NMR (400 MHz, $CDCl_3$): δ = 8.67 (s, 2H), 8.61 (s, 2H), 7.85 (d, J = 7.7 Hz, 4H), 7.60 (t, J = 7.7 Hz, 4H), 7.52 (t, J = 7.4 Hz, 2H), 3.31 (t, J = 7.9 Hz, 4H), 1.71 (quint, J = 7.8 Hz, 4H), 1.38–1.31 (m, 4H), 1.26–1.18 (m, 8H), 0.83 (t, J = 6.8 Hz, 6H) ppm. ^{13}C NMR (100 MHz, $CDCl_3$): δ = 143.2, 141.8, 136.6, 134.7, 131.0, 130.0, 129.3, 123.2, 120.7, 55.5, 31.0, 29.7, 27.8, 22.2, 13.9 ppm. Anal Calcd for $C_{34}H_{40}N_6O_4S_2$: *m*/*z* 661.2632 $[M + H]^+$. Found: MS (MALDI, CHCA): *m*/*z* 661.2638 $[M + H]^+$.

2.3.2.2. ***4,4′-[2,5-Bis(hexylsulfonyl)-1,4-phenylenebis(1H-1,2,3-triazole-4,1-diyl)]bis[N,N-dimethylbenzeneamine] 4ab.*** **3ab** (68.3 mg, 0.1 mmol, 1.0 eq) in 12.5 ml DCM (0.008 M) and 11.4 ml DMDO (0.035 M in acetone, 0.4 mmol, 4 eq). 73.5 mg (0.098 mmol, 98%) of **4ab** were obtained as a white solid. ^{1}H NMR (200 MHz, $CDCl_3$): δ = 8.67 (d, J = 1.7 Hz, 2H), 8.54 (d, J = 2.7 Hz, 2H), 8.27 (d, J = 8.8 Hz, 4H), 7.98 (d, J = 9.0 Hz, 4H), 3.77–3.47 (m, 16H), 2.17–2.00 (m, 4H), 1.61–1.46 (m, 4H), 1.40–1.29 (m, 4H), 0.88 (t, J = 6.7 Hz, 6H) ppm. ^{13}C NMR (100 MHz, $CDCl_3$): δ = 154.7, 146.7, 146.0, 136.7, 127.2, 124.4, 122.2, 121.0, 120.4, 63.4, 57.3, 31.4, 28.2, 23.2, 22.4, 14.0 ppm. Anal Calcd for $C_{38}H_{50}N_8O_4S_2$: *m*/*z* 747.3476 $[M + H]^+$. Found: MS (MALDI, CHCA): *m*/*z* 747.3497 $[M + H]^+$.

2.3.2.3. ***General polymerization procedure towards 6aa–bc.*** **1a–c** (1.0 eq) and **5a/b** (1.0 eq) were weighed in into separate vials on a high precision scale (d = 0.01 mg). CuI (0.1 eq), KF (3.0 eq) and H_2O (8.0 eq) were added to **1a–c** and the vial was sealed and flushed with argon. **5a–b** was dissolved in degassed THF/MeCN (4:1, 0.15 M) and added completely to the other reagents via a syringe. The reaction mixture was then heated to 100 °C (cooling while heating mode) in the microwave reactor for 6 h.

The solution was added dropwise to degassed methanol (1 ml per 0.015 mmol **1a–c**) using a syringe. The reaction vial was flushed with some degassed THF which was then also added to the degassed methanol. The precipitate was collected by vacuum filtration, dried in a constant flow of nitrogen, washed three times with water and twice with MeOH and again dried in a flow of nitrogen.

2.3.2.4. ***Poly[1H-1,2,3-triazole-4,1-diyl(9,9-dihexyl-9H-fluorene-2,7-diyl)-1H-1,2,3-triazole-1,4-diyl[2,5-bis(hexylthio)-1,4-phenylene]] 6aa.*** **1a** (377.23 mg, 0.750 mmol, 1.0 eq), CuI (14.3 mg, 0.075 mmol, 10 mol%), KF (130.7 mg, 2.25 mmol, 3.0 eq), H_2O (108.1 mg, 6.00 mmol, 8.0 eq), **5a** (312.42 mg, 0.750 mmol, 1.0 eq) and 5 ml THF/MeCN (4:1, 0.15 M) for 6 h at 100 °C (MW, cwh). Work-up according to the general procedure yielded 405.8 mg (70%) of the orange–brown solid **6aa**. ^{1}H NMR (200 MHz, $CDCl_3$): δ = 8.88–8.73 (br), 8.36–8.28 (br), 8.00–7.64 (br), 7.42–7.33 (br), 3.21–2.84 (br), 2.23–1.86 (br), 1.86–1.57 (br), 1.57–1.40 (br), 1.40–1.19 (br), 1.19–0.95 (br), 0.95–0.82 (br), 0.82–0.52 (br) ppm. GPC: M_n = 3.5 kDa, M_w = 7.5 kDa, PDI = 2.1.

2.3.2.5. ***Poly[1H-1,2,3-triazole-4,1-diyl(9,9-dihexyl-9H-fluorene-2,7-diyl)-1H-1,2,3-triazole-1,4-diyl[2,5-bis(hexylseleno)-1,4-phenylene]] 6ba.*** **1b** (298.38 mg, 0.500 mmol, 1.0 eq), CuI (9.5 mg, 0.050 mmol, 10 mol%), KF (87.2 mg, 1.50 mmol, 3.0 eq), H_2O (72.0 mg, 4.00 mmol, 8.0 eq), **5a** (208.28 mg, 0.500 mmol, 1.0 eq) and 3.3 ml THF/MeCN (4:1, 0.15 M) for 6 h at 100 °C (MW, cwh). Work-up according to the general procedure yielded 290.4 mg (67%) of the ocher solid **6ba**. ^{1}H NMR (200 MHz, $CDCl_3$): δ = 8.76–8.59 (br), 8.30–8.13 (br), 8.01–7.59 (br), 7.43–7.32 (br), 3.22–2.73 (br), 2.23–1.89 (br), 1.89–1.58 (br), 1.58–1.18 (br), 1.18–0.94 (br), 0.94–0.82 (br), 0.82–0.53 (br) ppm. GPC: M_n = 3.0 kDa, M_w = 6.6 - kDa, PDI = 2.2.

2.3.2.6. ***Poly[1H-1,2,3-triazole-4,1-diyl(9,9-dihexyl-9H-fluorene-2,7-diyl)-1H-1,2,3-triazole-1,4-diyl[2,5-bis(hexyltelluro)-1,4-phenylene]] 6ca.*** **1c** (277.62 mg, 0.400 mmol, 1.0 eq), CuI (7.6 mg, 0.040 mmol, 10 mol%), KF (69.7 mg, 1.20 mmol, 3.0 eq), H_2O (57.6 mg, 3.20 mmol, 8.0 eq), **5a** (166.62 mg, 0.400 mmol, 1.0 eq) and 2.7 ml THF/MeCN (4:1, 0.15 M) for 6 h at 100 °C (MW, cwh). Work-up according to the general procedure yielded 304.1 mg (79%) of the brown solid **6ca**. ^{1}H NMR: insufficient solubility for NMR measurement. GPC: M_n = 6.9 kDa, M_w = 14.3 kDa, PDI = 2.1 (measured in $CHCl_3$ due to low solubility in THF).

2.3.2.7. ***Poly[[9-(2-ethylhexyl)-9H-carbazole-3,6-diyl]-1H-1,2,3-triazole-1,4-diyl[2,5-bis(hexylthio)-1,4-phenylene]-1H-1,2,3-triazole-4,1-diyl] 6ab.*** **1a** (377.23 mg, 0.750 mmol, 1.0 eq), CuI (14.3 mg, 0.075 mmol, 10 mol%), KF (130.7 mg, 2.25 mmol, 3.0 eq), H_2O (108.1 mg, 6.00 mmol, 8.0 eq), **5b** (271.08 mg, 0.750 mmol, 1.0 eq) and 5 ml THF/MeCN (4:1, 0.15 M) for 6 h at 100 °C (MW, cwh). Work-up according to the general procedure yielded 443.9 mg (82%) of the yellow–orange solid **6ba**. ^{1}H NMR (200 MHz, $CDCl_3$): δ = 8.93–8.77 (br), 8.63–8.29 (br), 8.21–8.13 (br), 8.05–7.84 (br), 7.68–7.40 (br), 4.38–4.09 (br), 3.20–2.92 (br), 2.25–1.93 (br), 1.84–1.56 (br), 1.56–1.06 (br), 1.06–0.64 (br) ppm. GPC: M_n = 3.6 kDa, M_w = 7.2 kDa, PDI = 2.0.

2.3.2.8. ***Poly[[9-(2-ethylhexyl)-9H-carbazole-3,6-diyl]-1H-1,2,3-triazole-1,4-diyl[2,5-bis(hexylseleno)-1,4-phenylene]-1H-1,2,3-triazole-4,1-diyl].*** **1b** (298.38 mg, 0.500 mmol, 1.0 eq), CuI (9.5 mg, 0.050 mmol, 10 mol%), KF (87.2 mg, 1.50 mmol, 3.0 eq), H_2O (72.0 mg, 4.00 mmol, 8.0 eq), **5b** (180.72 mg, 0.500 mmol, 1.0 eq) and 3.3 ml THF/MeCN (4:1, 0.15 M) for 6 h at 100 °C (MW, cwh). Work-up according to the general procedure yielded 328.4 mg (81%) of the orange–brown solid **6bb**. ^{1}H NMR (200 MHz, $CDCl_3$): δ = 8.80–8.61 (br), 8.61–8.40 (br), 8.33–8.08 (br), 8.04–7.73 (br), 7.66–7.31 (br), 4.39–3.99 (br), 3.11–2.73 (br), 2.20–1.91 (br), 1.85–1.52 (br), 1.52–1.02 (br), 1.02–0.55 (br) ppm. GPC: M_n = 3.1 - kDa, M_w = 6.4 kDa, PDI = 2.1.

2.3.2.9. ***Poly[[9-(2-ethylhexyl)-9H-carbazole-3,6-diyl]-1H-1,2,3-triazole-1,4-diyl[2,5-bis(hexyltelluro)-1,4-phenylene]-1H-1,2,3-triazole-4,1-diyl] 6cb.*** **1c** (277.62 mg, 0.400 mmol, 1.0 eq), CuI (7.6 mg, 0.040 mmol, 10 mol%), KF (69.7 mg, 1.20 mmol, 3.0 eq), H_2O (57.6 mg, 3.20 mmol, 8.0 eq), **5b** (144.58 mg, 0.400 mmol, 1.0 eq) and 2.7 ml THF/MeCN (4:1, 0.15 M) for 6 h at 100 °C (MW, cwh). Work-up according to the general procedure yielded 261.3 mg (72%) of the orange–brown solid **6cb**. ^{1}H NMR/GPC: insufficient solubility for measurements.

2.3.2.10. ***General oxidation procedure for polymers 7aa and 7ab.*** **6aa**/**6ab** (1.0 eq) was dissolved in DCM (0.008 M). DMDO (0.035 M in acetone, 4.2 eq) was added dropwise and the solution stirred for 20 min at room temperature. Simple evaporation of the solvents yielded the desired products in sufficient purity.

2.3.2.11. ***Poly[1H-1,2,3-triazole-4,1-diyl(9,9-dihexyl-9H-fluorene-2,7-diyl)-1H-1,2,3-triazole-1,4-diyl[2,5-bis(hexylsulfonyl)-1,4-phenylene]] 7aa.*** **6aa** (116.3 mg, 1 eq) in 18.8 ml DCM (0.008 M) and 18.0 ml DMDO (0.035 M in acetone, 0.63 mmol, 4.2 eq). 125.6 mg (100%) of **7aa** were obtained as an orange–brown solid. ^{1}H NMR (200 MHz, $CDCl_3$): δ = 8.71–8.49 (br), 8.03–7.64 (br), 7.43–7.31 (br), 3.64–3.25 (br), 2.33–1.92 (br), 1.92–1.63 (br),

1.63–1.19 (br), 1.19–0.96 (br), 0.96–0.82 (br), 0.82–0.42 (br) ppm. GPC: M_n = 3.6 kDa, M_w = 8.3 kDa, PDI = 2.3.

2.3.2.12. ***Poly[[9-(2-ethylhexyl)-9H-carbazole-3,6-diyl]-1H-1,2,3-triazole-1,4-diyl[2,5-bis(hexylsulfonyl)-1,4-phenylene]-1H-1,2,3-triazole-4,1-diyl] 7ab.*** **6ab** (108.0 mg, 1 eq) in 18.8 ml DCM (0.008 M) and 18.0 ml DMDO (0.035 M in acetone, 0.63 mmol, 4.2 eq). 117.3 mg (100%) of **7ab** were obtained as a yellow–orange solid. ^{1}H NMR (200 MHz, $CDCl_3$): δ = 8.83–8.39 (br), 8.23–8.12 (br), 8.04–7.78 (br), 7.69–7.33 (br), 4.40–4.04 (br), 3.46–3.18 (br), 2.21–1.88 (br), 1.88–1.56 (br), 1.56–1.03 (br), 1.03–0.35 (br) ppm. GPC: M_n = 3.5 kDa, M_w = 7.5 kDa, PDI = 2.1.

3. Results and discussion

A continuous junction (CJ) design for organic electronic devices has the potential to significantly improve and simplify their production by applying just one organic material, which though enables post-processing modification to obtain different materials in a later production step. In the case of PSCs this means converting an electron donor (Fig. 1, gray) into an electron acceptor material (Fig. 1, black).

Reactive polymers are required to realize a device by this concept, but there are certain limitations to available reactions: a suitable reaction has to proceed fast, selective and without any nonvolatile byproducts, the electronic properties of the polymers have to be changed by the reaction and the reagent solvent should not wash away the processed polymer layer.

Oxidation of thioethers attached to a conjugated polymer backbone using dimethyldioxirane (DMDO) was found to perfectly suit these requirements. This organic reagent is commonly dissolved in acetone, which generally is a poor solvent for the considered functional polymers and which is also the volatile reaction byproduct [14]. Additionally, this reaction enables a severe modification of the intrinsic electronic properties by oxidation of electron-donating thioether groups (+M effect) to electron-withdrawing sulfoxides or sulfones (−M effect) [14], while simultaneously keeping the polymer backbone intact. With regard to applicability of DMDO, our group reported on a practical and efficient large-scale preparation of this oxidation reagent [9].

If a thioether substituted polymer thin layer is exposed to DMDO, an oxidation gradient within this layer is expected to occur; especially since oxidation of thioethers to sulfones proceeds stepwise via sulfoxides.

In addition to the exceptional prospects of applying DMDO to realize a continuous junction, sulfone substituted conjugated polymers – which are obtained by the post-polymerization modification – already gained previous interest as materials in PSCs. [15–17] The sulfone groups are described to "greatly lower both HOMO/LUMO levels, making these polymers potential electron acceptors (n-type) for polymeric electronic/optoelectronic applications" [15].

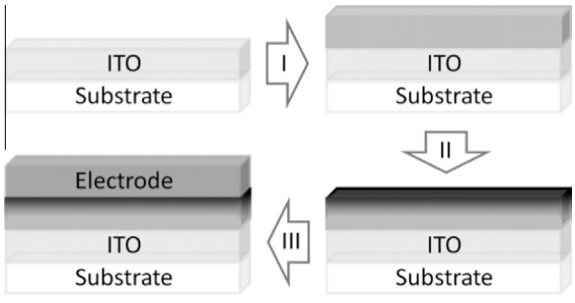

Fig. 1. Intended steps of device fabrication: printing or spin-coating of a donor polymer on a transparent electrode like indium tin oxide (ITO) (I), partial post-processing modification of the thin layer (II), application of the metal electrode (III).

In the following, the synthesis of model compounds and polymers suitable for modification using DMDO are discussed in detail. Modification using DMDO was successfully established in quantitative yields for both model compounds and polymers, which can be regarded as chemical proof of concept for the realization of a CJ design by the chosen reaction. Photophysical, electrochemical and electronic properties of the polymers are discussed in the final Sections 3.2.3 and 3.2.4 of this chapter.

3.1. Model compounds

Reaction conditions for the copper(I)-catalyzed azide–alkyne cycloaddition (CuAAC) polymerization were successfully optimized for the synthesis of model compounds **3aa–cb**. Copper(I) iodide served as a catalyst, while a good solvent for polymerizations – a 4:1 mixture of THF and acetonitrile – was applied. *In-situ* deprotection of the alkyne moieties by KF has been achieved. The reactions were carried out at moderate temperatures of 50 °C.

Purification by column chromatography proved to be difficult due to intense tailing. Therefore, crystallization was chosen for purification. However, this resulted in lower yields, although – according to TLC analysis – the reactions proceeded quantitatively within the reaction times given in Table 1.

The possibility of post-functionalization modification of the thioether groups using DMDO was demonstrated by the synthesis of compounds **4aa** and **4ab**. These reactions proceeded within seconds (according to TLC analysis) and resulted in quantitative yields without the need of further purification. Selenide and telluride analogs also were subject to oxidation, but did not yield any soluble products.

3.2. Polymers

3.2.1. Microwave-assisted polymerization

Polymerizations were first carried out under the pre-developed conditions for the reactions towards model compounds **3aa–cb**. Although polymerization was observed, the formation of higher molecular weights required reaction times of several days as was also reported for similar reactions in literature. [18] Leaving all other parameters unchanged but carrying out the polymerizations towards **6aa–cb** at elevated temperatures of 100 °C in a microwave reactor resulted in severely reduced reaction times of 6 h. Further reduction of the reaction times to 3 h only led to slightly lower molecular weights for the tested polymerizations towards **6aa** and **6ab** as shown in Table 2.

3.2.2. Post-polymerization modification

The conversion of a donor into an acceptor polymer (or a p-type into an n-type semiconductor) by post-polymerization modification is the key step towards the continuous junction (CJ) design for polymer solar cells (PSCs) and other organic electronic devices (Fig. 1, step II). Since the solvent for the oxidation of thioethers to sulfoxides and sulfones (Scheme 4) is acetone,

Table 1
Model compounds **3aa–cb**: reaction times and yields.

Model compound	Monomers		Reaction time (h)	Yield (%)
3aa	**1a**	**2a**	6	64
3ba	**1b**	**2a**	5	63
3ca	**1c**	**2a**	1	53
3ab	**1a**	**2b**	4	78
3bb	**1b**	**2b**	5	58
3cb	**1c**	**2b**	3	66

which is also the oxidation byproduct and exhibits a boiling point below 60 °C at ambient pressure, evaporation can readily be achieved.

Oxidized polymers **7aa** and **7ab** were obtained by post-polymerization modification of **6aa** and **6ab**. It is assumed that this reaction proceeds very fast, since oxidation of model compounds **3aa** and **3ab** was completed within seconds. Solvent evaporation yielded the desired polymers in quantitative yields.

The polymers were subject to ^{1}H NMR spectroscopy to verify oxidation. Both polymers, **7aa** and **7ab**, showed a significantly higher shift for the protons of the aliphatic side-chains which are closest to the sulfur atom. This is in accordance with the electron-withdrawing character of sulfone functionalities. A comparison of ^{1}H NMR spectra of non-oxidized and oxidized polymers is given in Fig. 2; the shifted protons are highlighted.

GPC measurements indicate no degradation of the polymers during oxidation (Table 3). The observed variations are within the limitations of this relative method for molecular weight determination.

As expected from experiments with the model compounds **3ba**, **3ca**, **3bb** and **3cb**, oxidation of selenide and telluride substituted polymers **6ba**, **6ca**, **6bb** and **6cb** did not afford any soluble polymers. However, this does not prevent selenium and tellurium groups from being used in polymers for future CJ devices. Solubility is a prerequisite for processing by printing or spin-coating, but is not required for a post-processing modification by DMDO and following fabrication steps.

3.2.3. Photophysical properties

Absorption spectra of polymer solutions (in dichloromethane) revealed a red-shift of the absorption maxima at around 300 nm from sulfide to selenide to telluride substituted polymers (Fig. 3). While for fluorene containing polymers **6aa–ca** this shift is rather large (~18 nm each), it is quite small for carbazole containing polymers **6ab–cb** (~6 nm each). Oxidation towards **7aa** and **7ab** did only result in minor changes in absorption spectra (Fig. 4).

Table 2
Polymers **6aa–cb**: GPC measurement results and yields; measurements carried out in THF (except for **6ca** ($CHCl_3$) due to poor solubility in THF).

Polymer	Monomers		M_n (kDa)	M_w (kDa)	PDI	Yield (%)
6aa	**1a**	**5a**	3.5	7.5	2.1	70
6aa (3h)	**1a**	**5a**	3.3	6.9	2.1	65
6ba	**1b**	**5a**	3.0	6.6	2.2	67
6ca	**1c**	**5a**	6.9	14.3	2.1	79
6ab	**1a**	**5b**	3.6	7.2	2.0	82
6ab (3h)	**1a**	**5b**	3.5	7.1	2.0	64
6bb	**1b**	**5b**	3.1	6.4	2.1	81
6cb	**1c**	**5b**	Insufficient solubility for GPC			72

Table 3
Comparison of GPC measurement results.

Polymer	M_n (kDa)	M_w (kDa)	PDI
6aa	3.5	7.5	2.1
7aa	3.6	8.3	2.3
6ab	3.6	7.2	2.0
7ab	3.5	7.5	2.1

Absorption spectra of polymer thin films deposited on fused silica substrates did not differ significantly from spectra recorded in solution (Supplementary material).

Photoluminescence measurements afforded two interesting results: First, emission intensities decrease rapidly by replacing sulfur by selenium and tellurium. In fact, we were not able to record proper emission spectra for polymers **6ba**, **6ca**, **6bb** and **6cb**. Secondly, a significant red-shift of the emission maxima by oxidation of polymers **6aa** and **6ab** was observed (Fig. 5). This shift is as big as 78 nm for carbazole containing polymer **6ab**, but is less pronounced for fluorene-based polymer **6aa** (35 nm). This corresponds to a shift of the emitted color from dark blue to yellow (**6ab** to **7ab**) and from blue to light blue (**6aa** to **7aa**) at an excitation wavelength of 366 nm (Fig. 6).

We attribute this enlarged Stokes shift to excited-state intramolecular charge-transfers. Dias et al. [19] described a similar observation for oligomers featuring sulfone moieties. They observed strong solvatochromic and thermochromic effects resulting in the conclusion that the molecules undergo intramolecular charge-transfer (ICT) reactions in the excited state. These ICT states are formed from local excited states and are stabilized by polar solvents, turning them into the lowest excited states.

This explanation of the observed shift of emission maxima of polymers **6aa–ab** by the introduction of push–pull systems by oxidation (and therefore making charge-transfers feasible) is in accordance with the marginal changes in the absorption spectra of the polymers. The observed red shift is assumed to result from a loss of energy by the stabilization of the ICT states. Although further experiments are required to confirm this theory, it also allows for an explanation of the severely larger red-shift for carbazole-based polymers compared to their fluorene-based analogs. The electron lone pair at the nitrogen, which also served as donor moiety in a previously described molecule featuring ICT [20], makes carbazoles considerably stronger electron donor units than fluorenes, which in turn facilitates intramolecular charge-transfers. In addition, the phenomenon of ICT has also been reported for 1,2,3-triazole linked materials recently [21,22].

Oxidation did not significantly affect the quantum yield of photoluminescence; measurements applying an Ulbricht sphere revealed only a marginal influence: Oxidation slightly increased the quantum yield from 13% (**6aa**) to 14% (**7aa**) and from 13%

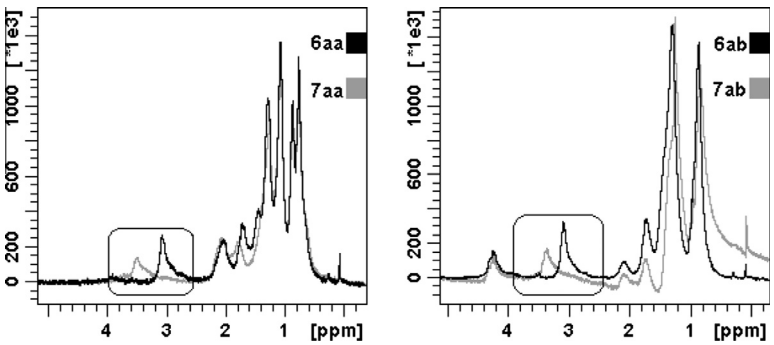

Fig. 2. Comparison of the aliphatic regions of ^{1}H NMR spectra: **6aa** and **7aa** (left), **6ab** and **7ab** (right).

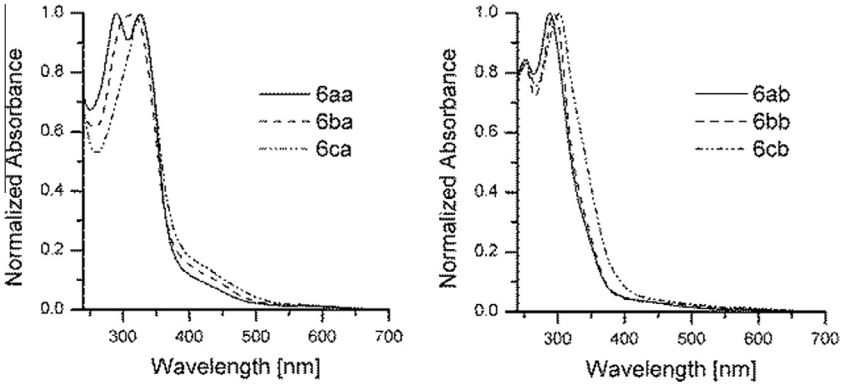

Fig. 3. Absorption spectra in dichloromethane: **6aa–ca** (left) and **6ab–cb** (right).

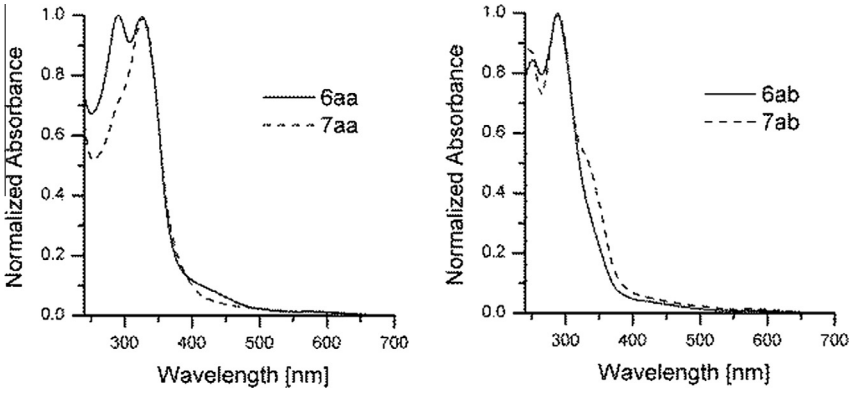

Fig. 4. Absorption spectra in dichloromethane: **6aa** and **7aa** (left), **6ab** and **7ab** (right).

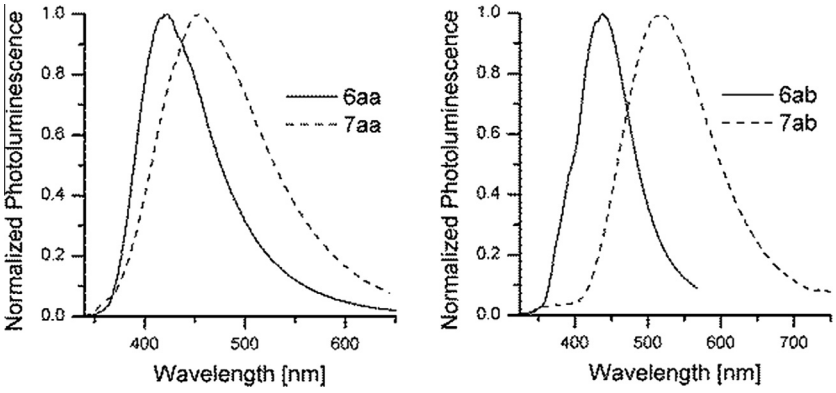

Fig. 5. Fluorescence spectra in dichloromethane: **6aa** and **7aa** (left), **6ab** and **7ab** (right).

(**6ab**) to 15% (**7ab**) at a concentration of 5 μM. Lower quantum yields were observed at higher concentrations (Table 4).

In dependence of the structural features these results suggest an application of post-polymerization modification using DMDO for color tuning in OLED fabrication. By this approach, materials of different emission wavelengths are available from the same starting polymer. Additionally, shifting the recombination zone in OLED devices by changing the applied voltage has been reported by different groups [23,24]. Thus, if the modification is performed after processing of the polymer (to obtain a CJ design), this may not only facilitate charge carrier injection, but could also allow for OLEDs with variable emission spectra in dependence of the applied voltage.

3.2.4. Electronic properties

The effect of oxidation of thioether substituents to sulfones on electronic properties of the polymers as well as the substitution of sulfide side groups by selenide moieties was investigated by cyclic voltammetry. Polymers featuring telluride substituents could not be examined in cyclic voltammetry experiments due to the poor solubility of the corresponding polymers.

For conductive polymers, the onset potential of oxidation E^{ox}_{onset} and reduction E^{red}_{onset} in films corresponds to the initial injection of holes and electrons to the HOMO and LUMO, respectively, and therefore correlates with the HOMO/LUMO levels [25]. The electrochemical energy gap evaluated from the onset potentials ($E^{EC}_g = E^{ox}_{onset} - E^{red}_{onset}$) is consequently related to the optical band

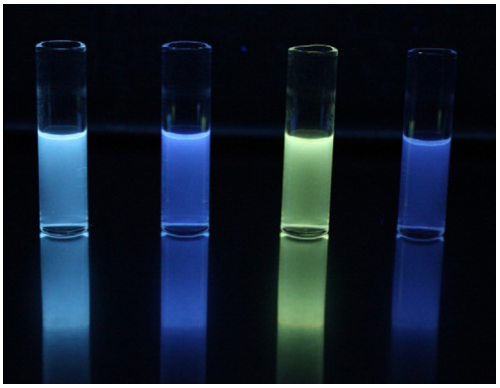

Fig. 6. Polymer solutions (50 μM (concentration of polymer repeating units) in dichloromethane) at an excitation wavelength of 366 nm, from left to right: **7aa**, **6aa**, **7ab**, **6ab**.

Table 4
Polymers **6aa**, **7aa**, **6ab**, **7ab**: excitation wavelength λ_{ex} for photoluminescence measurements, absorbance A (5 μM, d = 1 cm), molar extinction coefficient ε and photoluminescence quantum yield at different concentrations.

Polymer	λ_{ex} (nm)	A	ε [M^{-1} cm^{-1}]	PL quantum yield
6aa	333	0.249	49,800	13% (5 μM), 5% (50 μM), 3% (500 μM), 2% (5000 μM)
7aa	327	0.221	44,200	14% (5 μM), 8% (50 μM)
6ab	288	0.440	88,000	13% (5 μM), 4% (50 μM)
7ab	287	0.231	46,200	15% (5 μM), 6% (50 μM)

gap (E_g^{opt}), which can be determined from the absorption onset in optical spectra of polymer films [26,27].

Cyclic voltammetry measurements were performed on films in the range −2.0 V to 1.4 V vs Fc/Fc^+ for the determination of redox potentials and the estimation of HOMO/LUMO levels. All examined polymers exhibited oxidation waves with delayed reduction, which took place at more negative potentials, indicating chemical follow-up reactions occurring because of high reactivity of charged species formed during oxidation [28].

In contrast, reduction of the polymers was not observed since their reduction potentials were beyond the investigated potential window. This is in agreement with the optical band gap of the polymers being larger than 3 eV (Table 5). Therefore, the reduction onsets E_{onset}^{red}/LUMO levels were estimated from oxidation onsets E_{onset}^{ox}/HOMO levels using the correlation between the electrochemical and the optical bandgap (determined from the absorption onset of the polymer films; Supplementary material) [27].

Fig. 7 shows cyclic voltammograms of untreated polymers (**6aa** and **6ab**) and after treatment with DMDO (**7aa** and **7ab**). The voltammograms reveal that the oxidation onsets of oxidized polymers were positively shifted by about 0.35 V for fluorene-based polymers (Fig. 7, left) and by about 0.15 V for carbazole-based polymers (Fig. 7, right) compared to their untreated counterparts; suggesting a corresponding lowering of the HOMO levels (Table 5).

Since the oxidation of the sulfide groups did not affect the optical band gap of the polymers, the position of the LUMO level should consequently also be lowered by 0.4 eV and 0.2 eV, respectively, as result of oxidation (Table 5).

The substitution of sulfide side groups with selenides at the phenylene sub-units had only a small impact (0.1 eV) on the optical bandgap of fluorene- and carbazole-based polymers (Table 5). The oxidation onset was also only slightly affected by this substitution (see Fig. 8): a shift of 0.05 V to more negative potentials was observed for fluorene-based polymers (**6aa** and **6ba**), whereas a shift of 0.12 V to more positive potentials was recorded for carbazole-based polymers (**6ab** and **6bb**; Table 5).

Polymers **6ba** and **6bb** (selenide-substituted phenylene sub-units) exhibit practically the same position of HOMO level located at −5.59 eV and −5.57 eV, respectively. The polymer **6aa** (sulfide-substituted phenylene sub-units) has a somewhat lower position of the HOMO level (−5.64 eV) originating from the lower donor ability of S compared with Se. These similarities in HOMO levels indicate that the HOMO of the untreated pristine polymers is mainly located in the phenylene sub-units. The deviation in case of polymer **6ab** exhibiting a considerably higher HOMO level value of −5.45 eV than polymer **6aa** (−5.64 eV) is suggesting more complex interactions in this polymer. On oxidation, the location of the HOMO is shifted to fluorene/carbazole sub-units due to the higher donor ability in comparison to the sulfone-substituted moieties. Thus, the sulfone-substituted phenylene units determine the LUMO position of the oxidized polymers **7aa** and **7ab**.

The obtained photophysical and electrochemical data point out the expected and desired effect of lower HOMO and LUMO levels of oxidized polymers **7aa** and **7ab** compared to their non-oxidized counterparts **6aa** and **6ab**. Thus, a charge transfer between untreated polymers acting as electron donor and DMDO treated polymers acting as electron acceptor should be feasible. However, it is worth mentioning that the LUMO energy offsets of the polymers are only 0.4 eV and 0.2 eV, respectively. Assuming a similar exciton binding energy as in typical organic semiconductors, these values could be too low to allow for efficient exciton dissociation at the transition zone of one material to the other. Further work to improve the molecular design in order to increase the LUMO–LUMO offset is currently in progress.

Table 5
Polymers **6aa–bb**, **7aa** and **7ab**: electronic properties estimated from optical spectra and cyclic voltammograms.

Polymer	E_g^{opt} (eV)[a]	E_{ox} vs Fc/Fc^+ (V)[b]	Expected E_{red} vs Fc/Fc^+ (V)[c]	HOMO (eV)[d]	Expected LUMO (eV)[e]
6aa	3.2	0.84	−2.4	−5.64	−2.4
7aa	3.2	1.17	−2.0	−5.97	−2.8
6ab	3.2	0.65	−2.6	−5.45	−2.2
7ab	3.2	0.79	−2.4	−5.59	−2.4
6ba	3.1	0.79	−2.3	−5.59	−2.5
6bb	3.3	0.77	−2.5	−5.57	−2.3

[a] Optical bandgap determined from thin-film absorption onset, estimated error of ±0.1 eV.
[b] Oxidation onset determined against Fc/Fc^+ as internal standard, estimated error of ±0.02 V.
[c] $E_{red} \approx E_g^{opt} - E_{ox}$.
[d] Calculated from the equation: $E_{HOMO} = -(4.8 + E_{ox})$.
[e] $E_{LUMO} = -(4.8 + E_{red})$.

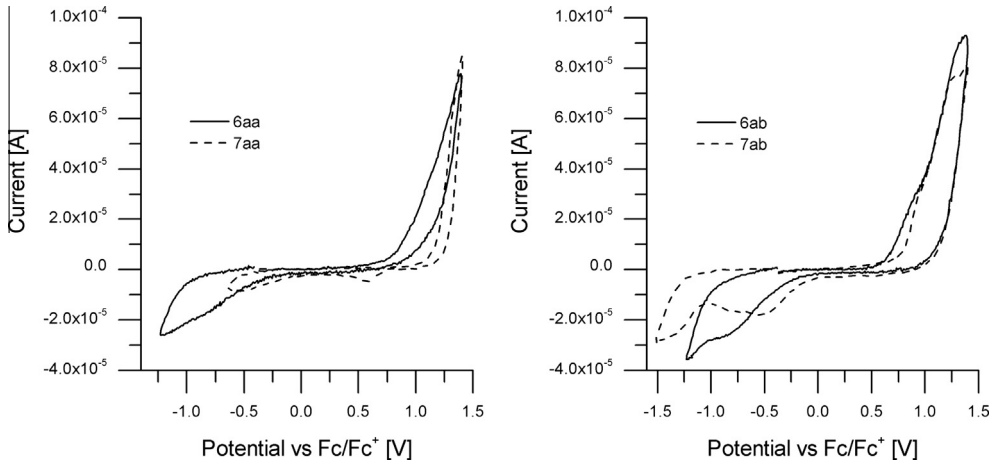

Fig. 7. Cyclic voltammograms of oxidation of fluorene-based polymers (left) and carbazole-based polymers (right), shown before (**6aa** and **6ab**) and after the treatment with DMDO (**7aa** and **7ab**) for comparison.

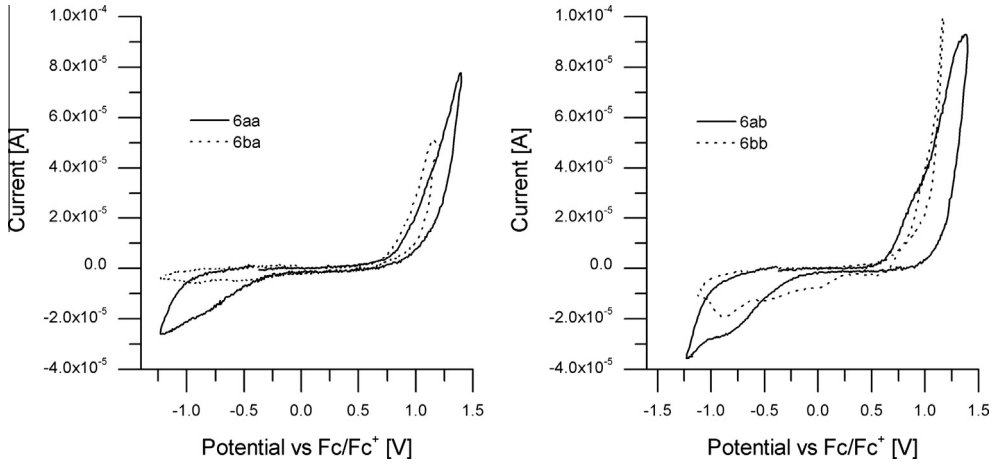

Fig. 8. Cyclic voltammograms of oxidation of fluorene-based polymers (left) and carbazole-based polymers (right) with sulfide (**6aa** and **6ab**) and selenide side groups (**6ba** and **6bb**) for comparison.

Characterization of organic field effect transistors (OFETs) employing the polymers investigated in this work did not reveal any current flow besides a small leakage current attributed to the low intrinsic conductivity of the silicon substrates (Supplementary material). Possible doping of the polymer layer by short exposure to air or annealing temperatures of up to 200 °C did not change this behavior (glass transition of 68 °C to 77 °C for polymers **6aa–bb** and **7aa** Supplementary material).

To further assess the suitability of the investigated polymers for organic electronic devices, polymer diodes with a layer stack of ITO–PEDOT:PSS–Polymer–Ca–Al were fabricated and characterized by IV-measurement from −1 V to +1 V. Again, no significant current flow could be observed. Under illumination, a small photoeffect could be observed, resulting in open circuit voltages in the range of 200–500 mV (Supplementary material). Short circuit currents and fill factors of the devices were negligible, however. In summary, due to the insufficient conductivity of the materials, which is attributed to both the molecular design (triazole moiety) and the degree of polymerization, it was not possible to derive electron or hole mobilities of the polymers. Aforementioned optimization of the molecular design also covers conductivity improvements for the target polymers.

4. Conclusions

In conclusion, the synthesis of the desired reactive polymers has been accomplished and the concept of post-polymerization oxidation has been demonstrated.

The photophysical and electrochemical characteristics of the target compounds indicate that the continuous junction concept is feasible by applying chalcogenide moieties as reactive sites for post polymerization modification. Cyclic voltammetry measurements confirm a lowering of both the HOMO and LUMO levels by oxidation of the sulfide groups with DMDO yielding the desired inversion of the electronic properties.

Although a LUMO–LUMO level difference of up 0.4 eV for the non-oxidized and the oxidized materials has been achieved ongoing investigations will focus on the enhancement of this off-set in order to improve exciton dissociation for potential OPV applications.

Acknowledgements

We gratefully thank Harald Wutzel (IAS) and Christian Bühler (FMF) for performing GPC measurements. Brigitte Holzer, Ernst Horkel and Christian Hametner (IAS) are acknowledged for NMR experiments. We also thank Michael Taubländer (IAS) for contrib-

uting to synthetic experiments and Paul Kautny (IAS) for DSC measurements and fruitful discussions.

Appendix A. Supplementary material

Supplementary data associated with this article can be found, in the online version, at http://dx.doi.org/10.1016/j.reactfunctpolym.2014.10.006.

References

[1] W. Brütting, J. Frischeisen, T.D. Schmidt, B.J. Scholz, C. Mayr, Phys. Status Solidi A 210 (2013) 44–65.
[2] N. Thejo Kalyani, S.J. Dhoble, Renew. Sustain. Energy Rev. 16 (2012) 2696–2723.
[3] D. Carsten, D. Vladimir, Rep. Prog. Phys. 73 (2010) 096401.
[4] B.C. Thompson, J.M.J. Fréchet, Angew. Chem. Int. Ed. 47 (2008) 58–77.
[5] G. Li, R. Zhu, Y. Yang, Nat. Photon. 6 (2012) 153–161.
[6] G. Chidichimo, L. Filippelli, Int. J. Photoenergy 2010 (2010).
[7] R. Pandey, R.J. Holmes, Adv. Mater. 22 (2010) 5301–5305.
[8] F. Glöcklhofer, D. Lumpi, B. Stöger, J. Fröhlich, New J. Chem. 38 (2014) 2229–2232.
[9] H. Mikula, D. Svatunek, D. Lumpi, F. Glöcklhofer, C. Hametner, J. Fröhlich, Org. Process Res. Dev. 17 (2013) 313–316.
[10] X. Guo, M. Baumgarten, K. Müllen, Prog. Polym. Sci. 38 (2013) 1832–1908.
[11] J.T. Simmons, J.R. Allen, D.R. Morris, R.J. Clark, C.W. Levenson, M.W. Davidson, L. Zhu, Inorg. Chem. 52 (2013) 5838–5850.
[12] K.D. Grimes, A. Gupte, C.C. Aldrich, Synthesis 9 (2010) 1441–1448.
[13] D. Li, X. Wang, Y. Jia, A. Wang, Y. Wu, Chin. J. Chem. 30 (2012) 861–868.
[14] M.E. González-Núñez, R. Mello, J. Royo, J.V. Ríos, G. Asensio, J. Am. Chem. Soc. 124 (2002) 9154–9163.
[15] C. Zhang, T.H. Nguyen, J. Sun, R. Li, S. Black, C.E. Bonner, S.-S. Sun, Macromolecules 42 (2009) 663–670.
[16] C. Zhang, J. Sun, R. Li, S. Black, S.-S. Sun, Synth. Met. 160 (2010) 16–21.
[17] T.H. Nguyen, C. Zhang, R. Li, S.-S. Sun, J. Polym. Sci. A Polym. Chem. 50 (2012) 1197–1204.
[18] Z. Chen, D.R. Dreyer, Z.-Q. Wu, K.M. Wiggins, Z. Jiang, C.W. Bielawski, J. Polym. Sci. A Polym. Chem. 49 (2011) 1421–1426.
[19] F.B. Dias, S. Pollock, G. Hedley, L.-O. Pålsson, A. Monkman, I.I. Perepichka, I.F. Perepichka, M. Tavasli, M.R. Bryce, J. Phys. Chem. B 110 (2006) 19329–19339.
[20] X. Peng, F. Song, E. Lu, Y. Wang, W. Zhou, J. Fan, Y. Gao, J. Am. Chem. Soc. 127 (2005) 4170–4171.
[21] M. Natali, M. Ravaglia, F. Scandola, J. Boixel, Y. Pellegrin, E. Blart, F. Odobel, J. Phys. Chem. C 117 (2013) 19334–19345.
[22] Y. Zhu, S. Guang, X. Su, H. Xu, D. Xu, Dyes Pigments 97 (2013) 175–183.
[23] P. Tyagi, R. Srivastava, A. Kumar, S. Tuli, M.N. Kamalasanan, J. Lumin. 136 (2013) 249–254.
[24] S.-S. Lee, D. Ko, C.-H. Chung, S.M. Cho, Synth. Met. 128 (2002) 51–55.
[25] S. Sensfuss, M. Al-Ibrahim, A. Konkin, G. Nazmutdinova, U. Zhokhavets, G. Gobsch, D.A.M. Egbe, E. Klemm, H.-K. Roth, Proc. SPIE 5215 (2004) 129–140.
[26] T. Johansson, W. Mammo, M. Svensson, M.R. Andersson, O. Inganas, J. Mater. Chem. 13 (2003) 1316–1323.
[27] Z. Fang, A.A. Eshbaugh, K.S. Schanze, J. Am. Chem. Soc. 133 (2011) 3063–3069.
[28] O. Yurchenko, D. Freytag, J. Phys. Chem. B 116 (2012) 30–39.